JOURNAL OF GENERAL VIROLOGY

RESEARCH ARTICLE

Ludwig-Begall *et al.*, *Journal of General Virology* 2020;101:510–522
DOI 10.1099/jgv.0.001406

MICROBIOLOGY SOCIETY

Replicative fitness recuperation of a recombinant murine norovirus – *in vitro* reciprocity of genetic shift and drift

Louisa F. Ludwig-Begall[1], Jia Lu[2]†, Myra Hosmillo[2], Edmilson F. de Oliveira-Filho[1,3], Elisabeth Mathijs[1,4], Ian Goodfellow[2], Axel Mauroy[1,5] and Etienne Thiry[1,*]

Abstract

Noroviruses are recognized as the major cause of non-bacterial gastroenteritis in humans. Molecular mechanisms driving norovirus evolution are the accumulation of point mutations and recombination. Recombination can create considerable changes in a viral genome, potentially eliciting a fitness cost, which must be compensated via the adaptive capacity of a recombinant virus. We previously described replicative fitness reduction of the first *in vitro* generated WU20-CW1 recombinant murine norovirus, RecMNV. In this follow-up study, RecMNV's capability of replicative fitness recuperation and genetic characteristics of RecMNV progenies at early and late stages of an adaptation experiment were evaluated. Replicative fitness regain of the recombinant was demonstrated via growth kinetics and plaque size differences between viral progenies prior to and post serial *in vitro* passaging. Point mutations at consensus and sub-consensus population levels of early and late viral progenies were characterized via next-generation sequencing and putatively associated to fitness changes. To investigate the effect of genomic changes separately and in combination in the context of a lab-generated inter-MNV infectious virus, mutations were introduced into a recombinant WU20-CW1 cDNA for subsequent DNA-based reverse genetics recovery. We thus associated fitness loss of RecMNV to a C7245T mutation and functional VP2 (ORF3) truncation and demonstrated individual and cumulative compensatory effects of one synonymous OFR2 and two non-synonymous ORF1 consensus-level mutations acquired during successive rounds of *in vitro* replication. Our data provide evidence of viral adaptation in a controlled environment via genetic drift after genetic shift induced a fitness cost of an infectious recombinant norovirus.

INTRODUCTION

Human noroviruses (HuNoVs) are recognized as major aetiologic agents of global sporadic and epidemic non-bacterial gastroenteritis [1], causing significant morbidity and mortality in developing countries [2] and high economic losses in developed countries [1, 3]. The development of HuNoV replicon bearing cells in a human hepatoma cell line [4], the B-cell culture system [5], the stem-cell-derived intestinal organoid system [6] and zebrafish larvae infection models [7] have all provided invaluable tools to dissect the NoV life cycle. However, there is still a lack of detailed understanding of HuNoV replication and significant questions remain unanswered due to the technical limitations of many of these experimental systems. The genetically and biologically closely related murine norovirus (MuNoV) combines the advantages of efficient *in vitro* culture systems [8, 9], availability of tools for genetic manipulation [10, 11] and easy *in vivo* infection of a genetically tractable native host [12] and thus remains the model of choice for NoV studies. Human noroviruses and MuNoVs [13] belong to the *Norovirus* genus within the *Caliciviridae* family of small, non-enveloped, positive sense,

Received 16 January 2020; Accepted 18 February 2020; Published 03 April 2020
Author affiliations: [1]Veterinary Virology and Animal Viral Diseases, Department of Infectious and Parasitic Diseases, FARAH Research Centre, Faculty of Veterinary Medicine, Liège University, Liège, Belgium; [2]Division of Virology, Department of Pathology, University of Cambridge, Cambridge, UK; [3]Institute of Virology, Charité-Universitätsmedizin Berlin, corporate member of Freie Universität Berlin, Humboldt-Universität zu Berlin, and Berlin Institute of Health, Berlin, Germany; [4]Infectious diseases in animals, Sciensano, Ukkel, Belgium; [5]Staff direction for risk assessment, Control Policy, FASFC, Brussels, Belgium.
***Correspondence:** Etienne Thiry, etienne.thiry@uliege.be
Keywords: Norovirus; murine; recombination; evolution; fitness; reverse genetics.
Abbreviations: HuNoV, Human norovirus; MuNoV, Murine norovirus; NoV, Norovirus; RecE, Virus progenies resulting from the first passage of RecMNV; RecL, Virus progenies resulting from the tenth passage of RecMNV; RecMNV, Viable recombinant MuNoV isolated by Mathijs *et al*, 2010 (29).
†Present address: The Babraham Institute, Babraham Hall House, Babraham, Cambridge, UK.
GenBank accession numbers for new sequence data: RecE: KU743153 and RecL: KU743152.
One supplememtary figure and two supplementary tables are available with the online version of this article.

single-stranded RNA viruses [14]. The linear, polyadenlyated 7.4–7.7 kb long HuNoV genome is classically organized into three ORFs, while MuNoV genomes are described to additionally harbour a fourth ORF [15, 16]. The 5′ proximal ORF1 encodes a large polyprotein that is co- and post-translationally cleaved into six non-structural viral proteins (NS1/2 to NS7) [17]. ORF2 and ORF3 encode the structural components of the virion, major and minor capsid protein, VP1 and VP2, respectively. ORF4, entirely overlapping the 5′end of ORF2, encodes a virulence factor (VF1) [18].

Replicative, transmissive, competitive and epidemiological fitness are key elements of the overall viral fitness [19], which conceptually determines how well a virus 'fits' into its environment [20]. Viral ecology is based on complex epigenetic and genetic interactions within the common triad of environment, host and virus. A given virus's ecology is thus governed in part by the particularities of its genetic evolution as it attempts to comply with the biological imperatives of genetic survival and replication [21]. Replicative fitness, defined as 'the capacity of a virus to produce infectious progeny in a given environment', can be investigated by either in *silico*, *in vitro*, *ex vivo* or *in vivo* experiments [19].

Molecular mechanisms mediating viral evolution are the accumulation of point mutations and recombination. While an accumulation of point mutations by virtue of the error-prone RNA-dependent RNA polymerase (RdRp) generally leads more gradually to the generation of quasispecies in RNA viruses [22–25], recombination can quickly create considerable changes in a viral genome, allowing for complete antigenic shifts, host jumps and both pathogenesis and fitness modifications [26]. A change of large genomic regions can highly impact the fitness of a novel recombinant virus, but can also provide the virus with new arms regarding its transmissive, competitive and epidemiological fitness [27].

While many field recombination events, predominantly at a typical ORF1/2 recombination breakpoint [28], have been detected *in silico* in the *Norovirus* genus [29, 30], few experimental data are available concerning NoV recombination under laboratory conditions and the mechanism(s) involved are poorly characterized [29]. The first *in vitro* experimental evidence of NoV recombination was provided by Mathijs *et al.* [31], describing the detection and isolation of a single viable recombinant virus from an infectious centre assay following coinfections of mouse leukaemic monocyte-macrophage cells (RAW264.7) with the two homologous parental MuNoV strains MNV1-CW1 and WU20 (87% nucleotide sequence similarity). The ensuing recombinant, RecMNV, composed of a WU20-related ORF1 and CW1-related ORFs 2, 3 and 4, was shown to exhibit reduced *in vitro* fitness compared to its parental strains [31], while nevertheless retaining *in vivo* infectivity (albeit also with a slight reduction of infectivity as measured by comparing weight loss, viral loads in faeces, blood and various organs of RecMNV infected mice) [32].

In the present study, we evaluated the replication capability of previously *in vitro*-generated recombinant MuNoV RecMNV at early (RecE) and late (RecL) stages of an *in vitro* replicative fitness adaptation experiment. We associated population-level genetic modifications to observable phenotypic profiles of viral fitness. Fitness loss of RecMNV was thus linked to a C7245T mutation and functional VP2 (ORF3) truncation; individual and cumulative compensatory effects of one non-synonymous VP1 (OFR2) and two NS1/2 synonymous ORF1 consensus level mutations acquired during successive rounds of *in vitro* replication were demonstrated, suggesting that interactions of viral proteins and/or RNA secondary structures of different ORFs may play a role in the regulation of replicative fitness post recombination. This *in vitro* model simulates the adaptation process (genetic drift) of NoVs after a recombination event (genetic shift); it supplements the scarce experimental data available concerning MuNoV recombination and may also further a conceptual understanding of the mechanisms behind HuNoV evolution.

METHODS

Viruses and cells

The murine macrophage cell line RAW264.7 (ATCC TIB-71) was maintained in Dulbecco's modified Eagle's medium (Invitrogen) containing 10% heat inactivated foetal calf serum (FCS) (BioWhittaker), 2% of an association of penicillin (5000 SI units ml^{-1}) and streptomycin (5 mg ml^{-1}) (PS, Invitrogen) and 1% 1 M HEPES buffer (pH 7.6) (Invitrogen) at 37 °C with 5% CO_2.

BHK cells engineered to express T7 RNA polymerase (BSR-T7 cells, obtained from Karl-Klaus Conzelmann, Ludwig Maximilian University, Munich, Germany) were maintained in DMEM containing 10% FCS, penicillin (100 SI units ml^{-1}) and streptomycin (100 µg ml^{-1}), and 0.5 mg ml^{-1} G418.

Murine NoV isolate RecMNV [31] was propagated in RAW264.7 cells as described by Mathijs *et al.* Initial RecMNV progeny was produced by infection of RAW264.7 cells at a m.o.i. (expressed as plaque-forming units per cell) of 0.05. Two days post-infection, cells and supernatant were harvested and clarified by centrifugation for 20 min at 1000 ***g*** after three freeze/thaw cycles (–80 °C alternating with 37 °C). Supernatants were purified by ultracentrifugation on a 30% sucrose cushion in a SW28 rotor (Beckman Coulter) at 23000 rounds per min for 2 h at 4 °C. Pellets were suspended in 500 µl PBS, aliquoted and frozen at –80 °C. Titres were determined via the $TCID_{50}$ method. For this, RAW 264.7 cells were seeded in 96-well plates, infected with tenfold serial dilutions of MuNoV, incubated for 4 days at 37 °C with 5% CO_2 and finally stained with 0.2% crystal violet for 30 min. The titres, expressed as $TCID_{50}$ ml^{-1}, were calculated according to the Reed and Muench transformation [33].

RecMNV *in vitro* serial replication

To evaluate the capability of replicative fitness adaptation of *in vitro*-generated recombinant MuNoV RecMNV in cell culture, RecMNV was serially replicated in RAW264.7 cells over nine passages. Briefly, monolayers of 5×10^6 RAW264.7 cells were initially infected with RecMNV at a m.o.i. of 0.05

and were incubated for 72 h. Following this, fresh RAW264.7 cell layers were infected with 100 µl supernatant from the preceding passage. The procedure was repeated eight times. The remaining supernatants were centrifuged at 1000 ***g*** for 20 min to remove cell debris and were stored at −80 °C until further analyses. Virus progenies resulting from the initial RecMNV production and those generated following the ninth passage of RecMNV are henceforth referred to as early (RecE) and late (RecL) recombinant progenies.

Plaque size analysis and replication kinetics of early (RecE) and late (RecL) RecMNV progenies

Two independent lysis plaque assays were performed in triplicate in RAW264.7 cells with RecE and RecL. Viral plaque sizes (15 discrete and well-isolated plaques were randomly selected per virus and per triplicate) of RecE and RecL were measured at 48 h p.i. with the open source image processing program ImageJ [34].

To compare infectivity between the progenies, a standardized production of RecE and RecL was performed. Per progeny, triplicate RAW264.7 monolayers in six-well plates were infected at a m.o.i. of 0.01 ($TCID_{50}$/cell). After 24 h p.i., total virus was released by three freeze/thaw cycles, clarified at 3000 r.p.m. for 20 min, and total viral progeny titres were analysed via $TCID_{50}$ (biological and technical triplicates).

Early (RecE) and late (RecL) RecMNV progenies sequence analysis

RNA was extracted from 150 µl of viral suspensions using the NucleoSpin RNA virus kit (Macherey-Nagel) according to the manufacturer's instructions. For genomic DNA depletion, the total RNA was treated with 4 MBU of Baseline-ZERO DNase (Epicentre) in a total volume of 60 µl. The reaction was incubated 15 min at 37 °C and inactivated by a bead-based purification step using the Agencourt AMPure XP (Beckman-Coulter). First-strand cDNA synthesis was performed using SuperScript IV reverse transcriptase (Thermo Fisher Scientific) according to the manufacturer's protocol. Briefly, 10 µl of DNase-treated total RNA was combined with oligonucleotide primers MNV-tail: TTTTTTTTTAAAATGC ATCTAACTACCAC (2.5 µM) and MNV-2745: CTCACGAT CAGCGAGGTAGTC (0.1 µM), dNTPs (10 mM: Promega) and nuclease-free water. Reactions were incubated at 65 °C for 10 min and cooled on ice for 5 min. A second reagent mix was added containing SuperScript IV enzyme (200 U: Thermo Fisher Scientific), RNasin Plus RNase Inhibitor (40 U: Promega), 0.1 M dTT (Thermo Fisher Scientific), before incubating at 50, 55 and 60 °C for 30 min, successively. A final incubation at 80 °C for 10 min was performed for inactivation. Second-strand synthesis was performed using NEBNext mRNA second-strand synthesis module (New England Biolabs) as per the manufacturer's instructions. The resulting dsDNA was purified using Agencourt AMPure XP (Beckman-Coulter) beads according to the manufacturer's instructions and samples eluted in 45 µl of nuclease-free water. Double-stranded cDNA samples were quantified using the Quantifluor dsDNA system (Promega) with the Quantus Fluorometer (Promega). One nanogram of each dsDNA sample was used to prepare sequencing libraries using the Nextera XT DNA Sample Preparation Kit (Illumina) according to the manufacturer's instructions. The libraries were quantified with the Kapa library quantification kit Illumina platforms (Kapa Biosystems) and the insertion size was verified using the Agilent Bioanalyzer with the high-sensitivity DNA kit (Agilent Technologies). Twenty-two libraries were multiplexed using standard Illumina indexing primers. Sequencing was performed using a MiSeq reagent kit version 3 (Illumina) with 2×300 bp paired-end sequencing on a MiSeq Benchtop Sequencer (Illumina).

Bioinformatics

The quality of the raw MiSeq sequence data of each library was assessed using FastQC v0.11.3 (http://www.bioinformatics.babraham.ac.uk/projects/). Trimming was performed using Trim galore! v0.3.8 (http://www.bioinformatics.babraham.ac.uk/projects/trim_galore/) based on quality (*Q* score >30) and length (length >80 bp, 5′ clip for R1 and R2=20). To obtain near full-length genomes for RecE and RecL, the trimmed reads were assembled *de novo* using SPAdes v3.9.0 with *k* values 21, 33, 55 and a subsample of 10000 or 13, 200 paired-end reads, respectively [35]. Reads from RecE and RecL were aligned to either the parental sequences MNV CW1 (GenBank accession number DQ285629) and WU20 (GenBank accession number EU004665.1) or each other using the Burrows–Wheeler Alignment tool (BWA) [36]. The alignments were sorted using Samtools v1.2 [37], converted using GATK v3.6.0 [38], and PCR duplicates were removed using Picard (http://broadinstitute.github.io/picard/). Subsequently variants were called using LoFreq [39].

Statistics

Statistical analyses of plaque size diameters determined with the Image J software were performed with SAS edition studio (SAS, Institute, Cary, NC, USA) using the NPAR1WAY procedure (non-parametric tests) or analysed using GraphPad Prism 7 (Graph-Pad Software) and *P*-values were determined with the non-parametric Mann–Whitney test, where $^{****}P<0.0001$, $^{***}P<0.001$, $^{**}P<0.01$, $^{*}P<0.05$, and ns is $P\geq0.05$.

GenBank accession numbers

The consensus nucleotide sequences of the near full genomes of RecE and RecL were deposited in GenBank/EMBL/DDBJ under the accession no. KU743153 and KU743152, respectively.

Generation of an inter-MNV chimeric plasmid

An inter-MNV chimeric cDNA was generated to contain a recombinant 'carbon copy' genome sequence ($RecMNV_{cc}$) of parental strains WU20 (before the recombination breakpoint) and CW1 (after the recombination breakpoint) under the control of a truncated T7 RNA polymerase promoter. Wherever SNPs were identified between RecE and its respective parental strains as encoded in GenBank, the position was

sequenced (post reverse transcription-PCR amplification) in the true, biological parental virus population to verify its presence or absence therein. If already present in a parental population, the mutation was considered to have been acquired prior to the recombination event in question (via genetic drift during generation of virus stocks) and was included in $RecMNV_{cc}$.

To build RecMNVcc, a WU20 insert obtained by PCR amplifying the WU20 ORF1 region from infectious virus stock was embedded into a pT7: MNV 3′Rz CW1 infectious clone backbone [40] containing a NotI restriction site in the m53 stem loop via Gibson assembly.

Generation of pT7: MNV 3′Rz M53 NotI

Briefly, to insert a *Not*I restriction site into pT7: MNV 3′Rz at the site of the m53 stem loop (GACCCCGC to GCGGCCGC at nt position 5024–5031), site-directed mutagenesis was performed by overlap mutagenic PCR with KOD Hot Start polymerase (Novagen) using primers IGUC3715 and 6042R (PCR1) and IGUC3716 and 3848F (PCR2) (see Table S1, available in the online version of this article). The resultant PCR products were used as templates for a third PCR with primers 3848F and 6042R to generate an amplicon containing the inserted *Not*I restriction site and flanked by *Afe*I and *Sac*II restriction sites. After *Afe*I and *Sac*II (New England Biolabs) digestion, the PCR3 product was ligated into *Afe*I- and *Sac*II-digested and dephosphorylated (Antarctic Phosphatase, New England Biolabs) pT7: MNV 3′Rz. The sequence of pT7: MNV 3′Rz N53NotI was confirmed using primers 3848F, 4450F and 6042R.

PCR amplification of WU20 ORF1

To enable the generation of an ORF1 WU20 cDNA, RNA was extracted from infectious virus stock (Epoch Life Science, EconoSpin All-in-One Mini Spin Columns), DNAse purified, and copied into oligo (d)T- and random hexamer-primed cDNA using SuperScript III (Invitrogen). Phusion high fidelity polymerase (New England Biolabs) was used to amplify a 5 kb region of WU20 cDNA, using 5′ primer IGUC3720 (containing the truncated T7 polymerase promoter sequence (of the pT7: MNV 3′Rz plasmid) and partial 5′ sequence of WU20) and 3′ primer IGUC3721 [containing the recombination site (sequence identity between WU20 and CW1)] (see Table S1).

Gibson assembly of pT7: MNV 3′Rz M53 NotI and WU20 ORF1

The pT7: MNV 3′Rz M53 NotI vector was cut with restriction enzymes *Ale*I and *Not*I-HF. A Gibson assembly (New England Biolabs) was set up with 100 ng gel purified vector and 200–300 ng column purified WU20 insert, according to the manufacturer's instructions. During the Gibson assembly process, the NotI site, previously inserted for cloning purposes, was removed. Following transformation into and recovery from NEB 5-alpha Gold Competent Cells (New England Biolabs), the identity of RecMNV was confirmed by sequencing with ten overlapping primer pairs covering the entire recombinant NoV genome (see Table S1). Three single nucleotide polymorphisms (SNPs) attributable either to PCR or cloning errors were corrected via site-directed mutagenesis to generate a perfect 'carbon copy' recombinant of parental strains WU20 and CW1.

Cloning of point mutations into a lab-generated inter-MNV chimeric plasmid

Following the generation of RecMNVcc, one consensus-level synonymous and three non-synonymous point mutations identified as entirely novel either to RecE or RecL populations (Table 1a, b, Fig. S1), were cloned into $RecMNV_{cc}$ via site-directed mutagenesis to generate five different mutant constructs, $RecE_{(C7245T)}$ (C7245T present in RecE and RecL), $RecMNV_{(C7245T\_T697C)}$ (T697C present in RecL), $RecMNV_{C7245T\_G234A}$ (G234A present in RecL), $RecMNV_{C7245T\_A5864G}$ (A5864G present in RecL), $RecL_{(C7245T\_G234A\_T697C\_A5864G)}$, in which unique RecE or RecL mutations were either isolated or combined. Insertion of the desired mutation was confirmed by sequencing. Details on the cloning strategy and primers used for the generation of the five different mutant constructs may be found in Table S2.

DNA-based reverse genetics to recover inter-MNV mutant viruses

Virus was rescued from the six RecMNV cDNA clones, wild-type pT7: MNV 3′Rz CW1 (as positive control) and the full-length cDNA clone of polymerase active site mutant pT7: MNV POL-3′Rz in which the NS7 active site is mutated from YGDD to YGGG (as replication-defective control) [41] by using the reverse genetics system based on recombinant fowlpox virus expressing T7 RNA polymerase, as previously described [10, 40]. Briefly, 1 µg of each cDNA expression construct was transfected, using Lipofectamine 2000 transfection reagent (Invitrogen), into BSR-T7 cells previously infected with recombinant fowlpox virus expressing T7 RNA polymerase at a m.o.i. of approximately 0.5 p.f.u. per cell (based on the virus titre in chick embryo fibroblasts). At 48 h post cDNA transfection, three freeze/thaw cycles at −80 °C/37 °C were performed to release virus particles from cells and infectious virus titres were determined as $TCID_{50}$ in RAW 264.7 cells using tenfold serial dilutions typically over a range of undiluted neat virus to 10^{-7}. The viral $TCID_{50}$ ml^{-1} of biological triplicates was determined by scoring signs of cytopathic effect (CPE) using microscopic visualization and crystal violet staining at 4 days post infection.

M.o.i.-controlled mid-point replication (P1) of inter-MNV mutant constructs

Mid-point passaging under standardized conditions [10 h infection, m.o.i. of 0.01 ($TCID_{50}$/cell)] of all six infectious recombinant constructs was carried out in RAW264.7 monolayers. To release infectious viruses of this first passage (P1) from cells, three freeze/thaw cycles were subsequently performed.

Table 1. Nucleotide changes present at consensus and sub-consensus level (under 50%) of the viral population of RecE (left), and RecL (right), as called using LoFreq and mapped against the parental strains, WU20 (GenBank: EU004665.1) and CW1 (GenBank: DQ285629.1), in ORF1/2 and ORF3, respectively. Positions corresponding to WU20 (left: nt 112 to 4865; right: nt 5290 to 7245) are shaded light grey; positions corresponding to CW1 (left: nt 5166 to 7354; right: nt 61 to 4961) are shaded dark grey

nt position	Parental strain	RecE	Raw depth	Frequency (%)
112	T	A	4126	99.95
193	T	A	7933	1.09
197	C	G	7996	1.06
198	G	C	8047	1.06
199	C	G	8020	1.05
203	T	A	8323	1.21
360	A	G	12743	1.08
697	T	C	14431	3.39
711	A	G	14072	1.94
829	C	T	14909	0.30
1039	A	G	14296	0.51
1503	A	G	16768	0.54
1683	A	G	17706	1.32
2030	C	A	18558	0.66
2269	A	G	20062	99.88
2532	T	C	18825	99.90
2804	C	G	12273	3.22
2978	C	T	12001	99.86
3164	C	T	12563	0.93
4607	T	C	18390	98.92
4865	A	G	18337	99.95
5166	C	T	16582	0.34
5461	C	T	16394	0.62
5484	C	T	15954	1.45
5502	T	G	15622	0.56
5613	C	T	15629	0.19
5664	C	T	15982	0.25
5864	A	G	11687	1.54
6089	A	G	16096	0.31
6117	T	C	15917	0.54
6458	T	C	19083	0.52
6534	C	A	20580	0.21
6610	A	G	21335	2.04
6625	C	T	21262	0.57
6630	C	T	21366	0.30
6676	C	T	21467	0.40
6677	A	G	21401	0.53
7245	C	T	9718	99.73
7354	C	T	1619	1.23
61	A	G	62	9.67
112	T	A	145	99.31
134	T	C	182	10.43
234	G	A	339	99.70
641	T	A	532	1.31
697	T	C	499	99.59
716	T	C	462	1.51
761	C	T	468	13.88
824	C	T	509	1.37
1077	A	G	565	1.76
1107	A	G	567	2.99
1540	A	G	708	1.55
1727	A	G	636	1.25
1995	G	T	710	2.53
2057	C	T	721	2.63
2211	A	G	814	2.08
2269	A	G	850	99.76
2498	C	T	106	1.32
2532	T	C	976	99.48
2643	C	T	658	2.73
2741	T	C	376	7.44
2978	C	T	376	100.00
2993	G	A	375	1.33
4097	C	G	538	8.55
4607	T	C	691	100.00
4727	A	G	742	1.48
4742	G	A	736	6.52
4865	A	G	657	99.84
4961	A	G	613	6.19
5290	C	T	542	1.84
5631	C	T	626	1.43

Continued

Table 1. Continued

nt position	Parental strain	RecE	Raw depth	Frequency (%)
5703	C	T	610	4.91
5864	A	G	432	72.22
6372	C	T	613	2.28
6510	G	A	703	2.27
6531	C	T	692	3.75
6534	C	A	697	4.87
6534	C	G	697	12.19
6657	A	G	720	1.52
7215	T	C	381	2.09
7245	C	T	330	99.69

Frequency: count (the number of times a particular nt occurs)/coverage.
nt: nucleotide.

Demonstration of VP2 functional truncation via Western blot

To analyse protein expression and specifically reveal VP2 functional truncation generated as a result of the C7245T mutation, BSR-T7 cells were harvested for Western blot analysis 48 h post-transfection with C7245T-mutated wild-type cDNA. Briefly, cells were lysed in RIPA buffer [50 mM Tris/HCl (pH 8.0), 150 mM NaCl, 1 mM EDTA, 1% Triton X-100, 0.1% SDS] and analysed subsequently by Western blot using a rabbit polyclonal antiserum to the minor capsid protein VP2 as described in [40].

Plaque size analysis and end-point replication kinetics of inter-MNV mutant constructs

To compare infectious virus titres of the six P1 inter-MNV constructs, $TCID_{50}$ assays were performed in RAW 264.7 cells using tenfold serial dilutions (as described above). Plaque assays were performed and analysed in RAW264.7 cells for each of the six constructs. Viral plaque sizes (25 discrete and well-isolated plaques were randomly selected per virus and per triplicate; i.e. n=75 plaques/virus) of each inter-MNV construct were measured at 48 h p.i. with the open source image processing program ImageJ.

RESULTS

Early and *in vitro* serially replicated late recombinant murine norovirus RecMNV progenies display differences in plaque sizes and replication kinetics

Differences of *in vitro* replicative fitness of RecMNV progeny RecE ('early'; prior to *in vitro* replication) and serially replicated, 'late' recombinant murine norovirus progeny RecL were analysed by comparing plaque sizes and replication kinetics. Plaque phenotypes showed that diameters of RecL were significantly larger (0.5 mm^2) than those of RecE (0.1 mm^2) (Fig. 1a). Standardized single-step replication of RecE and RecL and analysis of viral progenies via $TCID_{50}$ showed viral titres to differ by two orders of magnitude (2 log10) with mean values of $2.58\pm0.44\times10^5$ $TCID_{50}$ ml^{-1} for RecE and $1.00\pm0.55\times10^7$ $TCID_{50}$ ml^{-1} for RecL (Fig. 1b). Thus, both the plaque size analysis and standardized production of RecE and RecL progenies indicated a replicative fitness adaptation of RecMNV over intervening steps of viral amplification.

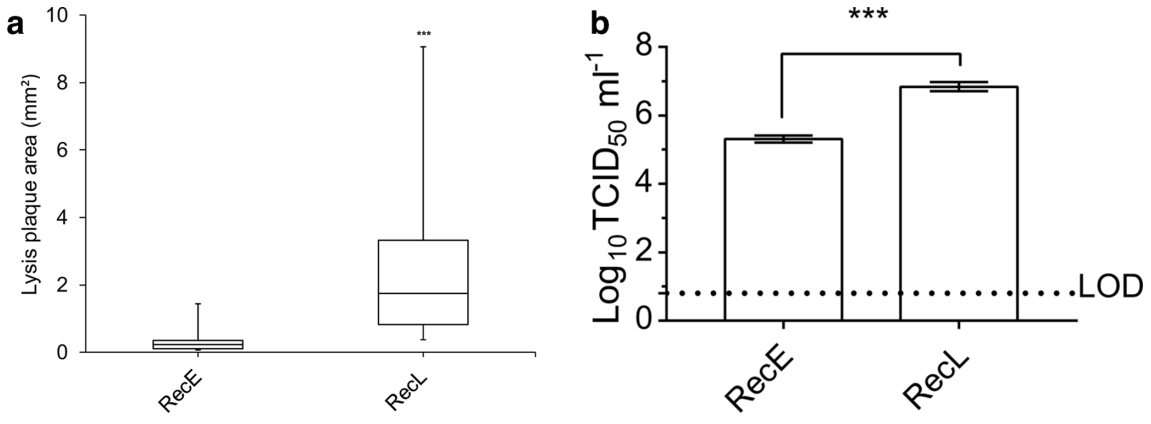

Fig. 1. Lysis plaque size comparison and analysis of viral progeny titres of RecE (a) and RecL (b). Plaque size quantification was performed on discrete, well-isolated plaques. The increase of mean surface area of the plaques from 0.1 to 0.5 mm^2, as determined with the Image J software and statistically analysed with procedure NPAR1WAY of SAS edition studio (SAS, Institute, Cary, NC, USA), is shown in (a). ***: P<0.001. Standardized production of RecE and RecL (infection of six-well plates at m.o.i. 0.01, 24 h incubation) and analysis of viral progeny titres via $TCID_{50}$ (biological and technical triplicates) shows viral titres differing by two orders of magnitude (2 log10) with mean values of $2.58\pm0.44\times10^5$ $TCID_{50}$ ml^{-1} reported for RecE and $1.00\pm0.55\times10^7$ $TCID_{50}$ ml^{-1} for RecL (b). P-values were computed by using a two-sided independent sample t-test. ***: P<0.001.

Next-generation sequencing (NGS) of early and late RecMNV progenies reveals a C7245T mutated VP2 in both populations and three further point mutations in the late RecMNV consensus sequence.

To associate differences in replicative fitness between RecE and RecL populations to changing molecular characteristics within the respective viral populations, MiSeq Illumina NGS was performed for RecE and RecL. Near-full-length, 7362 nucleotide-long consensus genomes were obtained by *de novo* assembly for RecE and RecL. The median read depth for both samples was at least 583 with 99.6% of the bases covered at least 20 times for RecE and 98.5% for RecL. These coverage rates allowed the confident detection of low-frequency single nucleotide variants [42]. The consensus sequence of RecE (GenBank accession number: KU743153) was compared to the corresponding sequences of its parental strains as encoded in GenBank. The recombination breakpoint was confirmed to be located at the ORF1/ORF2 junction in a 123 base pair large region of complete sequence identity (nucleotides 4968 to 5090) between the parental isolates. Thus, the complete RecE ORF1 sequences were matched against WU20 (GenBank: EU004665.1), while ORF2 and ORF3 sequences were compared to the corresponding regions of CW1 (GenBank: DQ285629.1) (Table 1). Wherever SNPs were identified at consensus level (over 50%) within the RecE population and its respective parental strains as encoded in GenBank, the position was sequenced in the original parental WU20 or CW1 virus population to verify its presence or absence therein. If already present in a parental population, the mutation must have been acquired prior to the recombination event in question (via genetic drift during generation of virus stocks) and was thus not included in further investigations. Accordingly, a single nucleotide transition from C (CW1) to T (RecE) at position 7245 was identified to have introduced a stop codon (Gln→Stop187) in ORF3, resulting in a 20 amino acid truncated VP2 in RecE (Table 2a, b).

The RecE consensus sequence was then mapped against that of RecL to identify mutations appearing between the two populations (and potentially associated the observed differences in replicative fitness) (Table 2a). A comparison of the consensus genome sequences of RecE and RecL (GenBank accession number: KU743152) revealed three nucleotide changes in total. Within NS1/2 (ORF1), two changes at positions 234 (G to A) and 697 (T to C) occurred, both of which resulted in amino acid mutations at positions 77 (Gly→Ser77) and 231 (Leu→Pro231), respectively (Table 2b). Interestingly, due to the non-silent mutation at nucleotide position 234, the RecL sequence corresponded to that of CW1 at the same position in both its nucleotide and amino acid sequence, reflecting the WU20 non-structural region 'picking up' a codon present in the corresponding region of CW1. ORF2 of RecL harboured a novel synonymous mutation at position 5864 (A to G), while the previous change at position 7245 was maintained in ORF3 of RecL.

The relative percentages of mutations (variants) within the population were determined after mapping the processed MiSeq Illumina sequencing reads to the respective reference sequence. Except at nucleotide positions 697 and 5864, variants hitherto reported were present at >98% within both populations and can confidently be viewed as stably established within the population. At position 697, 3.39% cytosine (C) and at nucleotide position 5864, 1.54% adenine (A) were present within the RecE population. Indicating a positive selection over the interim passages, these values mounted to 99.59 and 72.22%, respectively in RecL.

Table 2. Nucleotide changes (a) and non-synonymous mutations (b) between the consensus sequences of RecE, RecL and the parental strains WU20 and CW1. The relative percentages of mutations (variants) within the population were determined after mapping the processed MiSeq Illumina sequencing reads to the respective reference sequence, WU20 (GenBank: EU004665.1) in ORF1, CW1 (GenBank: DQ285629.1) in ORF2 and 3. Wherever deviating from the reference sequence, positions were sequenced in the respective WU20 or CW1 parental virus population. If already present in a parental population, the mutation was considered to have been acquired prior to the recombination event in question (via genetic drift during generation of virus stocks) and was not included in this table

	ORF1		ORF2	ORF3
	NS1/2			
nt position	234	697	5864	7245
WU20	G	T	A	C
CW1	A	T	A	C
RecE	**G**	**T**	A	**T**
RecL	**A**	**C**	G	**T**

	ORF1		ORF3
	NS1/2		
AA	77	231	190
WU20	Gly	Leu	Gln
CW1	Ser	Leu	Gln
RecE	Gly	Leu	Stop
RecL	Ser	Pro	Stop

Those changes resulting in a non-synonymous mutation (amino acid change) are marked in bold. The parental strain for the respective ORF is shaded in grey. Dotted underlining of nucleotides or amino acids signals changes appearing between the parental strain and RecE. Solid underlining of nucleotides or amino acids signals changes appearing between RecE and RecL. ORF: open reading frame; nt: nucleotide; AA: Amino acid.

Introduction of separate and combined RecMNV point mutations into an inter-MNV chimeric plasmid backbone via site-directed mutagenesis generates six chimeric plasmids

To investigate the effect of individual observed genomic changes within the RecE and RecL populations, an inter-MNV chimeric plasmid was generated by replacing the

ORF1 region of a CW1 cDNA (pT7: MNV 3'Rz [40]) with a PCR-amplified WU20 ORF1 to represent a recombinant 'carbon copy' ($RecMNV_{cc}$) of the parental strains. The unique consensus-level synonymous and three non-synonymous RecE or RecL point mutations identified in previous steps were introduced separately and in combination into $RecMNV_{cc}$ via site-directed mutagenesis, generating five different mutant constructs, $RecE_{(C7245T)}$ (C7245T present in RecE and RecL), $RecMNV_{(C7245T\_T697C)}$ (T697C present in RecL), $RecMNV_{C7245T\_G234A}$ (G234A present in RecL), $RecMNV_{C7245T\_A5864G}$ (A5864G present in RecL), $RecL_{(C7245T\_G234A\_T697C\_A5864G)}$. Insertion of the desired mutation was confirmed by sequencing.

DNA-based reverse genetics allows recovery of six infectious inter-MNV chimeric viruses

A DNA-based reverse genetics system allowed recovery of infectious virus (P0) at similar titres for all six recombinant constructs $RecMNV_{cc}$, $RecE_{(C7245T)}$ (C7245T present in RecE and RecL), $RecMNV_{(C7245T\_T697C)}$ (T697C present in RecL), $RecMNV_{C7245T\_G234A}$ (G234A present in RecL), $RecMNV_{C7245T\_A5864G}$ (A5864G present in RecL), $RecL_{(C7245T\_G234A\_T697C\_A5864G)}$ and wild-type MNV (Fig. 2) demonstrating that no mutation was so deleterious as to impair virus rescue.

A C7245T mutation results in functional truncation of VP2

The presumptive functional truncation of VP2 caused by the C7245T mutation in infectious viral progeny (passage 1) was confirmed via Western blot analysis using a rabbit polyclonal antiserum to the minor capsid protein VP2 as described in [40] (Fig. 3).

A replicative fitness cost of the C7245T VP2 truncation is compensated by separate and cumulative point mutations associated to late RecMNV

Mid-point passaging in RAW264.7 cells at low m.o.i. (0.01) of all six infectious recombinant constructs yielded a standardized passage 1 (P1) stock. Differences in *in vitro* replicative fitness of inter-MNV recombinant P1 progenies were compared using end-point replication kinetics and plaque size comparison and as proxy measurements. Titres of inter-MNV P1 viruses $RecMNV_{cc}$ ($1.36\pm0.08\times10^5$ $TCID_{50}$ ml^{-1}), $RecE_{(C7245T)}$ ($2.42\pm0.17\times10^4$ $TCID_{50}$ ml^{-1}) and $RecMNV_{C7245T\_T697C}$ ($2.42\pm0.08\times10^4$ $TCID_{50}$ ml^{-1}) differed by approximatively one order of magnitude (1 log10). Titres for $RecMNV_{C7245T\_G234A}$ ($7.65\pm0.17\times10^4$ $TCID_{50}$ ml^{-1}) and $RecMNV_{C7245T\_A5864G}$ ($1.36\times10^5\pm0.14$ $TCID_{50}$ ml^{-1}) were similar to that of $RecMNV_{cc}$, while the titre of $RecL_{(C7245T\_G234A\_T697C\_A5864G)}$ was slightly higher at $3.55\pm0.14\times10^5$ $TCID_{50}$ ml^{-1} (Fig. 4c).

The mean surface area of plaques [n=75 (3×25), biological triplicates; mm^2] was shown to differ significantly between the six constructs (Fig. 4b). $RecMNV_{cc}$ plaques were shown to have a mean surface area of $1.821\pm0.1708\,mm^2$, whilst $RecE_{(C7245T)}$ plaques were smaller by a factor of 3.9 ($0.465\pm0.08285\,mm^2$). Plaque sizes of $RecMNV_{C7245T\_G234A}$ (mean surface area $2.261\pm0.2197\,mm^2$; augmentation of plaque size by factor 1.2 as compared to $RecMNV_{cc}$) and $RecMNV_{C7245T\_A5864G}$ ($1.912\pm0.1903\,mm^2$) were shown to be similar to those of $RecMNV_{cc}$, and $RecMNV_{(C7245T\_T697C)}$ plaques with a mean surface area of $0.670\pm0.105\,mm^2$ displayed a factor 2.7 reduction of plaque size as compared to $RecMNV_{cc}$. The surface area of $RecL_{(C7245T\_G234A\_T697C\_A5864G)}$ plaques ($3.866\pm0.2482\,mm^2$) was shown to be 2.1 times larger than that of $RecMNV_{cc}$ plaques indicating a cumulative effect of three mutations in two different ORFs in RecL.

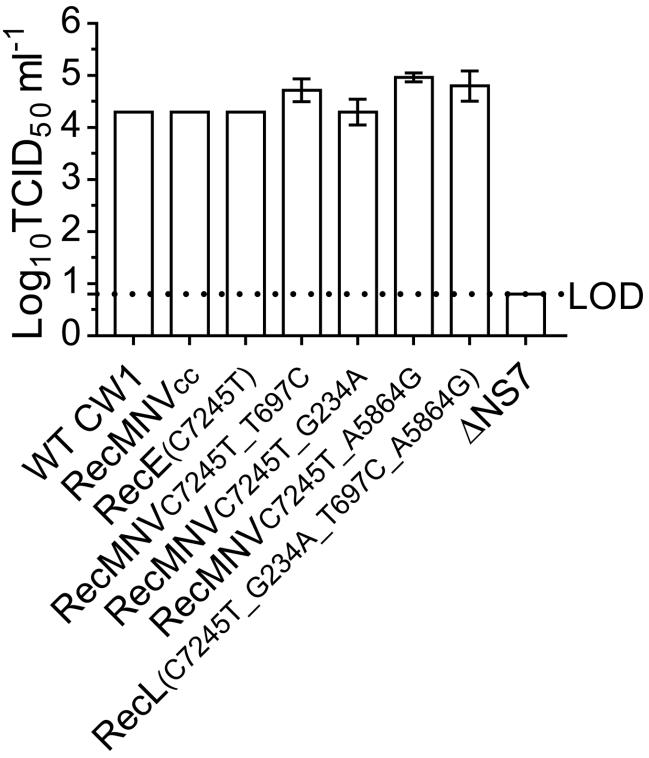

Fig. 2. A DNA-based reverse genetics system allowed recovery of infectious virus (P0) at similar titres for all six recombinant constructs, $RecMNV_{cc}$, $RecE_{(C7245T)}$, $RecMNV_{(C7245T\_T697C)}$, $RecMNV_{C7245T\_G234A}$, $RecMNV_{C7245T\_A5864G}$ and $RecL_{(C7245T\_G234A\_T697C\_A5864G)}$ and wild-type CW1. The mean log10 $TCID_{50}$ ml^{-1} and the standard error of the mean for each of the viruses are determined; formal statistical hypothesis testing, assuming independence between measurements of the infectivity of the wild-type and mutant viruses and computed by using two-sided independent sample *t*-tests showed no statistical differences between RecMNV mutants and WTCW1. WTCW1: plasmid pT7: MNV 3'Rz; ΔNS7: polymerase active site mutant pT7: MNV POL-3'Rz in which the NS7 active site is mutated from YGDD to YGGG.

DISCUSSION

This is the first study in which the capability of replicative fitness adaptation and associated genetic characteristics of a previously *in vitro*-generated recombinant MuNoV were evaluated at early and late time points of serial *in vitro* passaging. Our data provide evidence of viral adaptation to a controlled environment (here a cell-culture system) after a

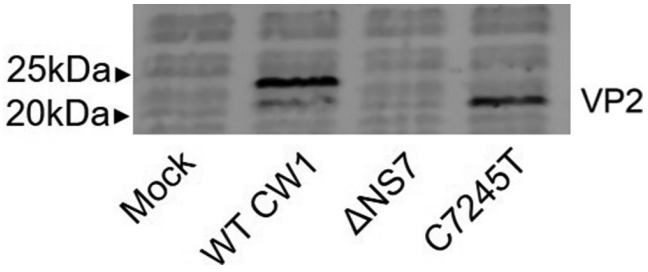

Fig. 3. The presumptive functional truncation of VP2 caused by the C7245T mutation in infectious viral progeny was confirmed via Western blot analysis using a rabbit polyclonal antiserum to the minor capsid protein VP2. The molecular ladder used was BioRad PrecisionPlus Dual colour. Mock: mock infection; WTCW1: plasmid pT7: MNV 3′Rz; ΔNS7: polymerase active site mutant pT7: MNV POL-3′Rz in which the NS7 active site is mutated from YGDD to YGGG.

recombination event, which initially induced a steep reduction of replication capacity [31, 32].

Recombination has previously been shown to incur fitness costs in viruses either as a result of disrupted epistatic interrelationships between the genetic loci of a novel recombinant (this typically between highly divergent viruses) [43] or as a result of point mutations acquired while bypassing the evolutionary bottleneck that is recombination. The recombinant strain RecMNV has been demonstrated to generate smaller plaques and have slower replication kinetics than its parental strains. Its lower replicative fitness was previously putatively associated to a longer cell sequestration before release [31].

Within compact viral genomes that encode only a few proteins, even single non-synonymous mutations can be sufficient to alter the structure or function of virus-encoded proteins to mediate fitness modifications [44, 45]. To investigate the origin of the reduced replicative fitness of RecMNV, i.e. RecE in this study, we investigated its genetic variant spectrum via MiSeq Illumina sequencing and matched its consensus sequence against those of its parental strains. The sole ORF1/2 recombination breakpoint [31] was confirmed, with ORF1 (NS1/2 to NS7) of RecE mapping against WU20, while ORFs 2 (VP1), 3 (VP2) and 4 (VF1) aligned homologously with CW1 sequences. A single C7245T point mutation and consequent introduction of a stop codon (Gln→Stop187) in ORF3 of RecE was shown to have caused a substantial functional truncation in the middle of a predicted VP2 stem-loop structure [46]. Minor capsid protein VP2, encoded by all caliciviruses, is located at the interior of the viral capsid and bound to a conserved motif in the shell domain of major capsid protein VP1. It is postulated to be involved in MuNoV encapsidation via an interaction with viral genomic RNA [17] and acidic regions of VP1 [47] and is held to regulate expression and stability of VP1 in HuNoVs [48]. Feline calicivirus VP2 forms a portal-like assembly following host cell receptor engagement [49]. VP2 integrity has previously been shown to be essential for productive replication of infectious feline calicivirus and attempts at producing infectious viruses after adding stop codons were previously unsuccessful [50]. To confirm the putative deleterious effect of point mutation C7245T in the context of a homologous recombinant background, albeit non-lethal, we implemented DNA-based reverse genetics to rescue both $RecMNV_{cc}$, an inter-MNV chimeric virus representing a perfect 'carbon copy' recombinant of parental WU20 and CW1 sequences, and $RecE_{(C7245T)}$, a $RecMNV_{cc}$ C7245T mutant. Plaque size comparison of inter-MNV chimeric viruses $RecMNV_{cc}$ and $RecE_{(C7245T)}$ indicated a deleterious effect of the C7245T mutation on replicative fitness of $RecE_{(C7245T)}$ viral progenies by a near factor four diminution of viral plaque sizes. Plaque size diameters are proportional to the number of cells that a virus lyses in a given time period. Their size is therefore related to virus productivity and cell-to-cell spread and their analysis is a well-established measure of viral fitness [19, 51–55]. The smaller lysis plaques of VP2 truncated RecE, indicating an inhibition of viral spread, are in line with the recent hypothesis that intact calicivirus VP2 functions as a channel for viral genome release from the endosome into the cytoplasm of a host cell [49]. A viral fitness cost was further confirmed by lower infectious titres of $RecE_{(C7245T)}$.

While initial imprecise recombination events present an evolutionary bottleneck and can induce a fitness cost, they may be followed by a stage of resolution optimizing viral fitness [43, 56]. We here report on a significant increase of plaque size between early and late progenies of recombinant MuNoV RecMNV, demonstrating a replicative fitness regain of the initially disadvantaged RecMNV after successive *in vitro* passaging. The fitness regain was additionally confirmed by differences in the kinetics of viral replication between RecE and RecL shown via a standardized virus production and supported by one-step and multi-step growth curve analyses. Titres of RecL at 24 h p.i. were two orders of magnitude (2 log10) higher than those of RecE and approached those of the parental strains at high m.o.i. To investigate the genetic changes that favoured the selection of viruses with faster replication kinetics and a large plaque phenotype, we obtained the near-complete genomic sequence of RecL. Comparison of RecE and RecL showed the C7245T mutation previously identified in RecE to be maintained in RecL. In addition, two non-synonymous nucleotide changes occurred within NS1/2 and a non-synonymous one in ORF2. NGS analysis allowed us to follow the evolution of RecMNV on a population level, showing not only the apparition of two of the variants at consensus level but also suggesting the positive selection and ultimate establishment of mutations initially represented at sub-consensus level within the population (T697C present at 3.39% in RecE and at 99.59% in RecL; A586G present at 1.54% in RecE and at 72.22% in RecL).

NS1/2, the least conserved NoV NS protein [47, 57], is involved in replication complex formation by associating with components of the endocytic and secretory pathway together with co-localizing NS4 [47, 58–60]. For MuNoVs, a single amino acid change in NS1/2 has been shown to induce a fitness gain in form of colonic tropism and persistence [61]. Here we demonstrate gain of replicative fitness in cell culture

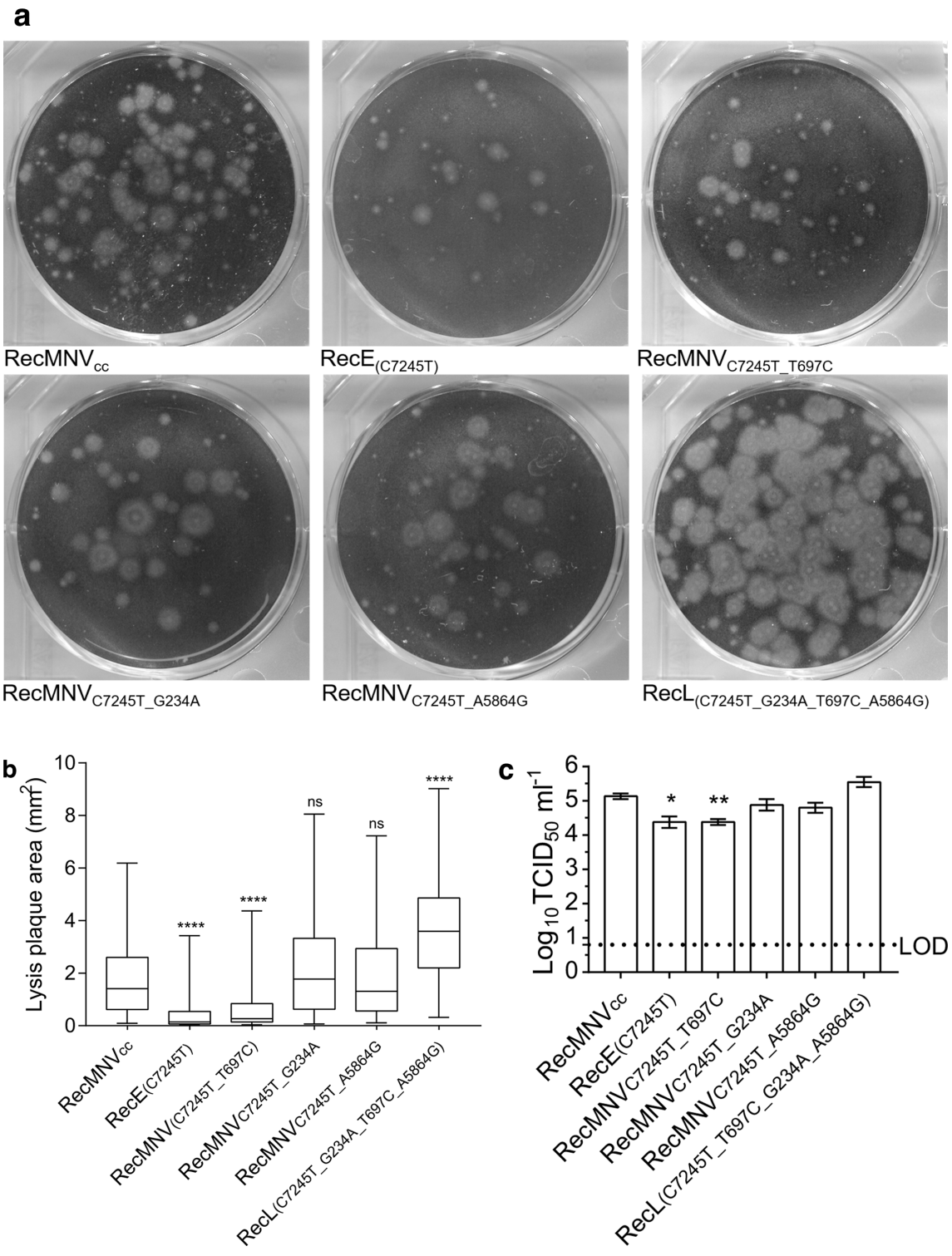

Fig. 4. Lysis plaque analysis, plaque size comparison and analysis of viral progeny titres of infectious inter-MNV chimeric viruses RecMNV$_{cc}$, RecE$_{(C7245T)}$, RecMNV$_{(C7245T_T697C)}$, RecMNV$_{C7245T_G234A}$, RecMNV$_{C7245T_A5864G}$ and RecL$_{(C7245T_G234A_T697C_A5864G)}$.

via acquisition of two non-synonymous NS1/2 mutations. Interestingly the 5′-proximal G234A mutation rescued the fitness cost mediated by 3′-proximal C7245T to higher levels than T697C. It has previously been demonstrated that physical interactions between the 5′ and 3′ ends of the NoV genomic RNA, which are sequence-mediated and further stabilized by cellular proteins, contribute to RNA circularisation and play a role in viral replication [62]. Sequence complementarity

has been shown to direct 5′–3′ end contacts; it is therefore intriguing that the C7245T mutation was followed by G234A, restoring complementarity (A-T to G-C) to a putative pairing.

In addition to non-synonymous mutations, synonymous mutations may also substantially impact viral fitness via non-neutral epistatic effects influencing RNA stability and splicing [20, 63] and silent tuning for increased adaptability [44, 64–66]. Since VP2 has been suggested to interact not only with the internal acidic domains of the calicivirus virion, but also with viral RNA [17, 50], the synonymous A5864G VP1 mutation is interesting in that it might have facilitated interactions between C7245T mutated VP2 and the viral genome.

To investigate the effect of the two non-synonymous NS1/2 mutations as well as the synonymous A5864G ORF2 (VP1) mutation on replication deficient $RecE_{(C7245T)}$, thus mimicking the natural genetic shift of RecMNV populations during serial passaging, inter-MNV chimeric viruses, $RecMNV_{C7245T\_G234A}$, $RecMNV_{(C7245T\_T697C)}$, $RecMNV_{C7245T\_A5864G}$ and $RecL_{(C7245T\_G234A\_T697C\_A5864G)}$, carrying individual and combined mutations were rescued via reverse genetics; the two previously described proxy measurements for replicative viral fitness indicated not only an augmentation of fitness for all three individual mutants but also a cumulative beneficial effect in which the replicative fitness of $RecMNV_{cc}$ was not only matched by $RecL_{(C7245T\_G234A\_T697C\_A5864G)}$ (as indicated by similar viral titres) but surpassed as regards lysis plaque size.

Additional factors such as the presence of different numbers of defective interfering particles can influence the fitness of different virus populations [67] and might have mediated differences between the RecE and RecL populations. This hypothesis was however not supported as Ct values for virus samples of similar titres obtained from a two-step RT qPCR analysis targeting the 5′-end of the MuNoV genome [31] were identical (results not shown).

Conclusion

Our results show that when a recombination event initially disadvantages a nascent chimeric NoV, an initial fitness cost precipitated by this genetic shift can be regained *in vitro* via genetic drift. Sporadic but regular emergence of HuNoV recombinant field strains may be explained with the help of this *in vitro* proof-of-concept model. *In vivo*, putative replicative disadvantages mediated by recombination events, can be compensated by other advantages at the level of competitive or the transmissive fitness (e.g. 'coat switching'), giving the virus time to regain its replicative fitness and even become dominant over its parental strains [29]. Indeed, for NoVs in the field the ability of the viral polymerase to switch templates at the start of ORF2 is considered advantageous, helping viruses to escape the evolutionary bottlenecks of host immune responses by the acquisition of a novel antigenic VP1 [30]; these recombinant viruses probably represent only subset of those that are actually generated, and are the ones that are maintained in the viral population after a rigorous functional selection and accumulation of adaptive point mutations. It is important to identify which parts of the genome are specifically prone to mediate fitness adaptation and to provide information for the production of effective detection and surveillance tools for the screening of emerging NoV strains, including recombinant ones. This study may serve as a starting point for the further development of *in vitro* HuNoV recombination studies in robust cell-culture systems to allow generation and detection of recombinants and elucidation of as yet unresolved mechanics of NoV recombination.

Funding information
This work was supported by grants from the Fund Leon Fredericq for biomedical research at the University Hospital of Liège (L.F.L-B.), the German Academic Exchange Service (L.F.L-B.), the Fédération Wallonie-Bruxelles (Bourse d'excellence WBI.World – SOR/2017/332396) (L.F.L.-B.), the Service Publique Fédéral 'Santé Publique, Sécurité de la Chaîne alimentaire et Environnement' (RT15/8 IQUINOR2) (L.F.L.-B, A.M., E.T.), the F.R.S.-FNRS (Research Credit 33703738) (L.F.L.-B., E.T.), the CNPq Brazilian National Council for Scientific and Technological Development (E.F.O.F.), and was further funded by research grants to IG: Wellcome Trust Ref: 207498/Z/17/Z. I.G. is a Wellcome trust Senior Fellow.

Acknowledgements
We thank Lorène Dams, Barbara Toffoli, Elisabetta Di Felice and Orkun Ozhelvaci for their technical assistance as well as Steven Van Borm and Frank Vandenbussche for their contribution to the full genome sequencing performed in this work.

Conflicts of interest
The authors declare that there are no conflicts of interest.

References

1. Robilotti E, Deresinski S, Pinsky BA. Norovirus. *Clin Microbiol Rev* 2015;28:134–164.
2. Patel MM, Widdowson M-A, Glass RI, Akazawa K, Vinjé J *et al*. Systematic literature review of role of noroviruses in sporadic gastroenteritis. *Emerg Infect Dis* 2008;14:1224–1231.
3. Bartsch SM, Lopman BA, Ozawa S, Hall AJ, Lee BY. Global economic burden of norovirus gastroenteritis. *PLoS One* 2016;11:e0151219–16.
4. Chang K-O, Sosnovtsev SV, Belliot G, King AD, Green KY. Stable expression of a Norwalk virus RNA replicon in a human hepatoma cell line. *Virology* 2006;353:463–473.
5. Jones MK, Grau KR, Costantini V, Kolawole AO, de Graaf M *et al*. Human norovirus culture in B cells. *Nat Protoc* 2015;10:1939–1947.
6. Ettayebi K, Crawford SE, Murakami K, Broughman JR, Karandikar U *et al*. Replication of human noroviruses in stem cell-derived human enteroids. *Science* 2016;353:1387–1393.
7. Van Dycke J, Ny A, Conceição-Neto N, Maes J, Hosmillo M *et al*. A robust human norovirus replication model in zebrafish larvae. *PLoS Pathog* 2019;15:e1008009–1008021.
8. Wobus CE, Thackray LB, Virgin HW. Murine norovirus: a model system to study norovirus biology and pathogenesis. *J Virol* 2006;80:5104–5112.
9. Wobus CE, Karst SM, Thackray LB, Chang K-O, Sosnovtsev SV *et al*. Replication of norovirus in cell culture reveals a tropism for dendritic cells and macrophages. *PLoS Biol* 2004;2:e432.
10. Arias A, Bailey D, Chaudhry Y, Goodfellow I. Development of a reverse-genetics system for murine norovirus 3: long-term persistence occurs in the caecum and colon. *J Gen Virol* 2012;93:1432–1441.
11. Yunus MA, Chung LMW, Chaudhry Y, Bailey D, Goodfellow I. Development of an optimized RNA-based murine norovirus reverse genetics system. *J Virol Methods* 2010;169:112–118.
12. Karst SM, Wobus CE, Lay M, Davidson J, Virgin HW. Stat1-Dependent innate immunity to a Norwalk-like virus. *Science* 2003;299:1575–1578.

13. Scipioni A, Mauroy A, Vinjé J, Thiry E. Animal noroviruses. *Vet J* 2008;178:32–45.
14. Clarke IN, Estes MK, Green KY, Hansman G, Knowles NJ *et al*. *Virus Taxonomy: Classification and Nomenclature of Viruses: Ninth Report of the International Committee on Taxonomy of Viruses*. San Diego: Elsevier; 2012.
15. Karst SM, Zhu S, Goodfellow IG. The molecular pathology of noroviruses. *J Pathol* 2015;235:206–216.
16. Karst SM, Wobus CE, Goodfellow IG, Green KY, Virgin HW. Advances in norovirus biology. *Cell Host Microbe* 2014;15:668–680.
17. Thorne LG, Goodfellow IG. Norovirus gene expression and replication. *J Gen Virol* 2014;95:278–291.
18. McFadden N, Bailey D, Carrara G, Benson A, Chaudhry Y *et al*. Norovirus regulation of the innate immune response and apoptosis occurs via the product of the alternative open reading frame 4. *PLoS Pathog* 2011;7:e1002413.
19. Wargo AR, Kurath G. Viral fitness: definitions, measurement, and current insights. *Curr Opin Virol* 2012;2:538–545.
20. Lauring AS, Andino R. Quasispecies theory and the behavior of RNA viruses. *PLoS Pathog* 2010;6:e1001005–1001008.
21. Hurst C, Lindquist HDA. *Defining the Ecology of Viruses*. Cincinnati: Academic Press; 2000.
22. Andino R, Domingo E. Viral quasispecies. *Virology* 2015;479-480:46–51.
23. Boon D, Mahar JE, Abente EJ, Kirkwood CD, Purcell RH *et al*. Comparative evolution of GII.3 and GII.4 norovirus over a 31-Year period. *J Virol* 2011;85:8656–8666.
24. Mauroy A, Scipioni A, Mathijs E, Ziant D, Daube G *et al*. Genetic and evolutionary perspectives on genogroup III, genotype 2 bovine noroviruses. *Arch Virol* 2014;159:39–49.
25. Mauroy A, Taminiau B, Nezer C, Ghurburrun E, Baurain D *et al*. High-Throughput sequencing analysis reveals the genetic diversity of different regions of the murine norovirus genome during in vitro replication. *Arch Virol* 2017;162:1019–1023.
26. Simon-Loriere E, Holmes EC. Why do RNA viruses recombine? *Nat Rev Microbiol* 2011;9:617–626.
27. Pérez-Losada M, Arenas M, Galán JC, Palero F, González-Candelas F. Recombination in viruses: mechanisms, methods of study, and evolutionary consequences. *Infect Genet Evol* 2015;30:296–307.
28. Bull RA, Hansman GS, Clancy LE, Tanaka MM, Rawlinson WD *et al*. Norovirus recombination in ORF1/ORF2 overlap. *Emerg Infect Dis* 2005;11:1079–1085.
29. Ludwig-Begall LF, Mauroy A, Thiry E. Norovirus recombinants: recurrent in the field, recalcitrant in the lab – a scoping review of recombination and recombinant types of noroviruses. *J Gen Virol* 2018;99:970–988.
30. Bull RA, Tanaka MM, White PA. Norovirus recombination. *J Gen Virol* 2007;88:3347–3359.
31. Mathijs E, Muylkens B, Mauroy A, Ziant D, Delwiche T *et al*. Experimental evidence of recombination in murine noroviruses. *J Gen Virol* 2010;91:2723–2733.
32. Mathijs E, Oliveira-Filho EFde, Dal Pozzo F, Mauroy A, Thiry D *et al*. Infectivity of a recombinant murine norovirus (RecMNV) in BALB/cByJ mice. *Vet Microbiol* 2016;192:118–122.
33. Reed LJ, Muench H. A simple method of estimating fifty percent endpoints. *Am J Hyg*;27.
34. Schneider CA, Rasband WS, Eliceiri KW, Instrumentation C. Nih image to ImageJ: 25 years of image analysis. *Nat Methods* 2012;9:671–675.
35. Bankevich A, Nurk S, Antipov D, Gurevich AA, Dvorkin M *et al*. SPAdes: a new genome assembly algorithm and its applications to single-cell sequencing. *J Comput Biol* 2012;19:455–477.
36. Li H, Durbin R. Fast and accurate short read alignment with Burrows-Wheeler transform. *Bioinformatics* 2009;25:1754–1760.
37. Li H, Handsaker B, Wysoker A, Fennell T, Ruan J *et al*. The sequence Alignment/Map format and SAMtools. *Bioinformatics* 2009;25:2078–2079.
38. McKenna A, Hanna M, Banks E, Sivachenko A, Cibulskis K *et al*. The genome analysis toolkit: a MapReduce framework for analyzing next-generation DNA sequencing data. *Genome Res* 2010;20:1297–1303.
39. Wilm A, Aw PPK, Bertrand D, Yeo GHT, Ong SH *et al*. LoFreq: a sequence-quality aware, ultra-sensitive variant caller for uncovering cell-population heterogeneity from high-throughput sequencing datasets. *Nucleic Acids Res* 2012;40:11189–11201.
40. Chaudhry Y, Skinner MA, Goodfellow IG. Recovery of genetically defined murine norovirus in tissue culture by using a fowlpox virus expressing T7 RNA polymerase. *J Gen Virol* 2007;88:2091–2100.
41. Thorne L, Lu J, Chaudhry Y, Bailey D, Goodfellow I. Targeting macrophage- and intestinal epithelial cell-specific microRNAs against norovirus restricts replication in vivo. *J Gen Virol* 2018;99:1621–1632.
42. Olson ND, Lund SP, Colman RE, Foster JT, Sahl JW *et al*. Best practices for evaluating single nucleotide variant calling methods for microbial genomics. *Front Genet* 2015;6:1–15.
43. Sackman AM, Reed D, Rokyta DR. Intergenic incompatibilities reduce fitness in hybrids of extremely closely related bacteriophages. *PeerJ* 2015;3:e1320.
44. Elde NC. Poliovirus evolution: the strong, silent type. *Cell Host Microbe* 2012;12:605–606.
45. Borin BN, Tang W, Nice TJ, McCune BT, Virgin HW *et al*. Murine norovirus protein nS1/2 aspartate to glutamate mutation, sufficient for persistence, reorients side chain of surface exposed tryptophan within a novel structured domain. *Proteins* 2014;82:1200–1209.
46. Bailey D, Karakasiliotis I, Vashist S, Chung LMW, Reese J *et al*. Functional analysis of RNA structures present at the 3' extremity of the murine norovirus genome: the variable polypyrimidine tract plays a role in viral virulence. *J Virol* 2010;84:2859–2870.
47. Thorne L, Bailey D, Goodfellow I. High-Resolution functional profiling of the norovirus genome. *J Virol* 2012;86:11441–11456.
48. Bertolotti-Ciarlet A, Crawford SE, Hutson AM, Estes MK. The 3' end of Norwalk virus mRNA contains determinants that regulate the expression and stability of the viral capsid protein VP1: a novel function for the VP2 protein. *J Virol* 2003;77:11603–11615.
49. Conley MJ, McElwee M, Azmi L, Gabrielsen M, Byron O *et al*. Calicivirus VP2 forms a portal-like assembly following receptor engagement. *Nature* 2019;565:377–381.
50. Sosnovtsev SV, Belliot G, Chang K-O, Onwudiwe O, Green KY. Feline calicivirus VP2 is essential for the production of infectious virions. *J Virol* 2005;79:4012–4024.
51. Wasik BR, Bhushan A, Ogbunugafor CB, Turner PE. Delayed transmission selects for increased survival of vesicular stomatitis virus. *Evolution* 2015;69:117–125.
52. Abedon ST, Culler RR. Optimizing bacteriophage plaque fecundity. *J Theor Biol* 2007;249:582–592.
53. Brandon Ogbunugafor C, Alto BW, Overton TM, Bhushan A, Morales NM *et al*. Evolution of increased survival in RNA viruses specialized on cancer-derived cells. *Am Nat* 2013;181:585–595.
54. Domingo E. *Viral Fitness as a Measure of Adaptation*, 1st ed; 2016.
55. Muylkens B, Meurens F, Schynts F, de Fays K, Pourchet A *et al*. Biological characterization of bovine herpesvirus 1 recombinants possessing the vaccine glycoprotein E negative phenotype. *Vet Microbiol* 2006;113:283–291.
56. Lowry K, Woodman A, Cook J, Evans DJ. Recombination in enteroviruses is a biphasic replicative process involving the generation of greater-than genome length 'imprecise' intermediates. *PLoS Pathog* 2014;10:e1004191.
57. Lateef Z, Gimenez G, Baker ES, Ward VK. Transcriptomic analysis of human norovirus NS1-2 protein highlights a multifunctional role in murine monocytes. *BMC Genomics* 2017;18:39.

58. **Hyde JL**, **Mackenzie JM**. Subcellular localization of the MNV-1 ORF1 proteins and their potential roles in the formation of the MNV-1 replication complex. *Virology* 2010;406:138–148.
59. **Kaiser WJ**. Analysis of protein-protein interactions in the feline calicivirus replication complex. *J Gen Virol* 2006;87:363–368.
60. **Bailey D**, **Kaiser WJ**, **Hollinshead M**, **Moffat K**, **Chaudhry Y** *et al*. Feline calicivirus P32, p39 and p30 proteins localize to the endoplasmic reticulum to initiate replication complex formation. *J Gen Virol* 2010;91:739–749.
61. **Nice TJ**, **Strong DW**, **McCune BT**, **Pohl CS**, **Virgin HW**. A single-amino-acid change in murine norovirus nS1/2 is sufficient for colonic tropism and persistence. *J Virol* 2013;87:327–334.
62. **López-manríquez E**, **Vashist S**, **Ureña L**, **Goodfellow I**, **Chavez P** *et al*. Norovirus genome circularization and efficient replication are facilitated by binding of PCBP2 and hnRNP A1. *J Virol* 2013;87:11371–11387.
63. **Draghi JA**, **Parsons TL**, **Wagner GP**, **Plotkin JB**. Mutational robustness can facilitate adaptation. *Nature* 2010;463:353–355.
64. **Lauring AS**, **Acevedo A**, **Cooper SB**, **Andino R**. Codon usage determines the mutational robustness, evolutionary capacity and virulence of an RNA virus. *Cell Host Microbe* 2012;12:623–632.
65. **Chamary JV**, **Parmley JL**. Hearing silence: non-neutral evolution at synonymous sites in mammals. *Nat Rev Genet* 2006;7:98–108.
66. **Wilke CO**, **Drummond DA**. Signatures of protein biophysics in coding sequence evolution. *Curr Opin Struct Biol* 2010;20:385–389.
67. **Thompson KAS**, **Yin J**. Population dynamics of an RNA virus and its defective interfering particles in passage cultures. *Virol J* 2010;7:257.